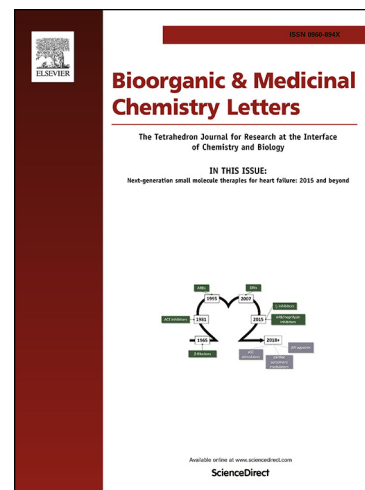


Accepted Manuscript

Discovery of a Class of Highly Potent Janus Kinase 1/2 (JAK1/2) Inhibitors Demonstrating Effective Cell-Based Blockade of IL-13 Signaling

Mark Zak, Emily J. Hanan, Patrick Lupardus, David G. Brown, Colin Robinson, Michael Siu, Joseph P. Lyssikatos, F. Anthony Romero, Guiling Zhao, Terry Kellar, Rohan Mendonca, Nicholas C. Ray, Simon C. Goodacre, Peter H. Crackett, Neville McLean, Christopher A. Hurley, Po-wai Yuen, Yun-Xing Cheng, Xiongcai Liu, Marya Liimatta, Pawan Bir Kohli, Jim Nonomiya, Gary Salmon, Gerry Buckley, Julia Lloyd, Paul Gibbons, Nico Ghilardi, Jane R. Kenny, Adam Johnson



PII: S0960-894X(19)30217-3
DOI: <https://doi.org/10.1016/j.bmcl.2019.04.008>
Reference: BMCL 26375

To appear in: *Bioorganic & Medicinal Chemistry Letters*

Received Date: 11 November 2018
Revised Date: 27 March 2019
Accepted Date: 3 April 2019

Please cite this article as: Zak, M., Hanan, E.J., Lupardus, P., Brown, D.G., Robinson, C., Siu, M., Lyssikatos, J.P., Romero, F.A., Zhao, G., Kellar, T., Mendonca, R., Ray, N.C., Goodacre, S.C., Crackett, P.H., McLean, N., Hurley, C.A., Yuen, P-w., Cheng, Y-X., Liu, X., Liimatta, M., Kohli, P.B., Nonomiya, J., Salmon, G., Buckley, G., Lloyd, J., Gibbons, P., Ghilardi, N., Kenny, J.R., Johnson, A., Discovery of a Class of Highly Potent Janus Kinase 1/2 (JAK1/2) Inhibitors Demonstrating Effective Cell-Based Blockade of IL-13 Signaling, *Bioorganic & Medicinal Chemistry Letters* (2019), doi: <https://doi.org/10.1016/j.bmcl.2019.04.008>

This is a PDF file of an unedited manuscript that has been accepted for publication. As a service to our customers we are providing this early version of the manuscript. The manuscript will undergo copyediting, typesetting, and review of the resulting proof before it is published in its final form. Please note that during the production process errors may be discovered which could affect the content, and all legal disclaimers that apply to the journal pertain.

Discovery of a Class of Highly Potent Janus Kinase 1/2 (JAK1/2) Inhibitors Demonstrating Effective Cell-Based Blockade of IL-13 Signaling.

Mark Zak^{a,*}, Emily J. Hanan^a, Patrick Lupardus^a, David G. Brown^b, Colin Robinson^b, Michael Siu^a, Joseph P. Lyssikatos^a, F. Anthony Romero^a, Guiling Zhao^a, Terry Kellar^a, Rohan Mendonca^a, Nicholas C. Ray^b, Simon C. Goodacre^b, Peter H. Crackett^b, Neville McLean^b, Christopher A. Hurley^b, Po-wai Yuen^c, Yun-Xing Cheng^c, Xiongcai Liu^c, Marya Liimatta^a, Pawan Bir Kohli^a, Jim Nonomiya^a, Gary Salmon^b, Gerry Buckley^b, Julia Lloyd^b, Paul Gibbons^a, Nico Ghilardi^a, Jane R. Kenny^a, Adam Johnson^a.

^a Genentech Inc., 1 DNA Way, South San Francisco, California 94080, USA

^b Charles River Laboratories, 8-9 Spire Green Centre, Harlow, Essex, CM19 5TR, United Kingdom

^c Pharmaron Beijing Co. Ltd., 6 Taihe Road, BDA, Beijing 100176, PR China

* Corresponding Author. E-mail address: mzak@gene.com. Phone: 650-467-4533

Abstract

Disruption of interleukin-13 (IL-13) signaling with large molecule antibody therapies has shown promise in diseases of allergic inflammation. Given that IL-13 recruits several members of the Janus Kinase family (JAK1, JAK2, and TYK2) to its receptor complex, JAK inhibition may offer an alternate small molecule approach to disrupting IL-13 signaling. Herein we demonstrate that JAK1 is likely the isoform most important to IL-13 signaling. Structure-based design was then used to improve the JAK1 potency of a series of previously reported JAK2 inhibitors. The ability to impede IL-13 signaling was thereby significantly improved, with the best compounds exhibiting single digit nM IC₅₀'s in cell-based assays dependent upon IL-13 signaling. Appropriate substitution was further found to influence inhibition of a key off-target, LRRK2. Finally, the most potent compounds were found to be metabolically labile, which makes them ideal scaffolds for further development as topical agents for IL-13 mediated diseases of the lungs and skin (for example asthma and atopic dermatitis, respectively).

Keywords

Janus Kinase, JAK, JAK1, JAK2, interleukin-13, IL-13, structure-based design, asthma, atopic dermatitis

ACCEPTED MANUSCRIPT

The Janus kinases (JAKs) are a family of four intracellular tyrosine kinases (JAK1, JAK2, JAK3, and TYK2) that regulate the JAK/STAT signaling pathway.¹ The JAK/STAT cascade is initiated when signaling molecules known as cytokines bind to the extracellular domains of their transmembrane receptor complexes. The JAKs associate with the intracellular domains of the cytokine receptors and become phosphorylated and activated upon cytokine binding. Subsequently, an additional family of intracellular proteins known as the signal transducers and activators of transcription (STATs) become phosphorylated. Once phosphorylated the STATs dimerize and translocate to the cell nucleus where they control genes relevant to a range of biological functions including immunity, inflammation, and hematopoiesis. The JAKs are attractive drug targets because they can be effectively inhibited by small molecules, and because inhibiting JAKs can block the cellular effects of the cytokines that signal through them.

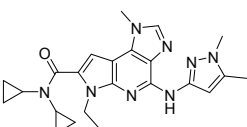
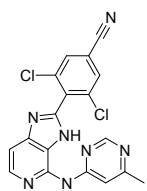
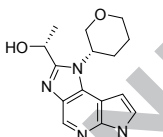
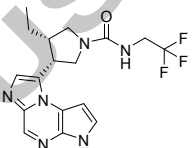
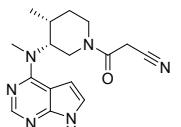
One important cytokine signaling through JAK/STAT is interleukin-13 (IL-13). IL-13 is implicated in allergic inflammation, thus interrupting its signaling via JAK inhibition may provide benefit in associated diseases such as severe asthma and atopic dermatitis.² Many cytokines recruit and activate multiple JAK isoforms in their receptor complexes. In the case of IL-13 three isoforms, namely JAK1, JAK2, and TYK2 are activated.³ However, it is known that not all the JAKs associated with a given cytokine's receptor complex play an equal role in controlling the downstream signaling. IL-6, for example, is another cytokine that recruits and activates JAK1, JAK2, and TYK2. Notably, selective JAK1 inhibition can effectively block IL-6 signaling, whereas inhibition of JAK2 and TYK2 appear to play only a minor role.⁴

To assess the relative importance of JAK1, JAK2, and TYK2 kinase activity on IL-13 signaling, we tested a panel of inhibitors with different JAK family selectivity profiles in an IL-13 triggered cell-based assay (Table 1). IL-13 signals through its receptor complex and associated JAKs,

converting inactive and unphosphorylated STAT6 to the active and phosphorylated form (pSTAT6). Thus, our IL-13-pSTAT6 cell-based assay involved stimulating BEAS-2B cells⁵ with IL-13, and monitoring for pSTAT6 formation in the presence or absence of JAK inhibitor.⁶ During assay benchmarking we wished to minimize the potential for poor cell penetrance to limit cell-based potency of test compounds. As such we, chose highly characterized JAK inhibitors (**1** – **5**)^{7,8,9,10,11} with both potent activity in cell-based assays dependent on the JAK isoforms they inhibit, and moderate to high permeability in MDCK transwell assays (Table 1). Compound **1** is a highly biochemically potent and selective JAK2 inhibitor that also shows potent inhibition in a JAK2-dependent cell-based assay (SET-2 IC₅₀ = 60 nM). Despite potent cellular engagement of JAK2, we found that **1** showed negligible inhibition in our IL-13-pSTAT6 assay, indicating that JAK2 inhibition is not likely to be effective in disrupting IL-13 signaling. Similarly, **2** is a potent and selective TYK2 inhibitor that previously showed strong inhibition in a TYK2-dependent cell-based assay (IL-23-pSTAT3 IC₅₀ = 66 nM). Despite potent cellular TYK2 engagement, compound **2** exhibited only very weak cellular inhibition in our IL-13-pSTAT6 assay, indicating that TYK2 inhibition is also not likely to be effective in disrupting IL-13 signaling. Also notable is the fact that both compounds **1** and **2** are highly permeable in the MDCK transwell assay, making it unlikely that poor cell penetrance is responsible for the poor IL-13-pSTAT6 potency. In contrast with the selective JAK2 (**1**) and TYK2 (**2**) inhibitors, compounds with potent biochemical JAK1 inhibition (**3**, **4**, **5**) exhibited correspondingly potent inhibition in our IL-13-pSTAT6 assay. Indeed, disruption of cell-based IL-13 signaling appeared to track consistently with JAK1 biochemical potency regardless of potency against the other JAK isoforms. Notably, compounds **2** – **5** possess markedly different selectivity profiles for JAK1 relative to the other JAK family members, yet in each case the IL-13-pSTAT6 IC₅₀ was remarkably proportional to the biochemical

JAK1 K_i (IL-13-pSTAT6 $IC_{50} \div$ JAK1 $K_i = 50x - 71x$). The consistent correlation between IL-13-pSTAT6 IC_{50} and JAK1 K_i , coupled with the negligible disruption in IL-13 signaling by potent JAK2 (1) or TYK2 (2) inhibitors led us to believe that JAK1 inhibition likely played the dominant role in disrupting IL-13 signaling, while JAK2 and TYK2 were likely less important.

Table 1. Biochemical and cell-based JAK inhibition, and MDCK permeability of previously reported JAK inhibitors.

				
Compound name: BMS-911543 (1)	G-444 (2)	G-989 (3)	Upadacitinib (4)	Tofacitinib (5)
JAK isoform(s) most potently inhibited: JAK2	TYK2	JAK1	JAK1	JAK1, JAK3, JAK2
Reported progression status: Ph1/2a clinical trials	Preclinical in vivo tool compound	Preclinical in vivo tool compound	Ph3 clinical trials	Approved drug

Ex	^a Literature Data			^b Data Generated in This Work						
	Cell-Based Assay Name	Primary JAK Involved	Cell-Based IC_{50} (nM)	^c MDCK A:B, B:A÷A:B	^d JAK1 K_i (nM)	^e JAK2: JAK1	^f JAK3: JAK1	^g TYK2: JAK1	IL-13-pSTAT6 IC_{50} (nM)	^h IL-13-pSTAT6 $IC_{50} \div$ JAK1 K_i
1	SET-2	JAK2	60	16, 0.94	360	0.0013x	ⁱ 0.31x	^j 0.11x	^k >1000	^l NC
2	IL-23-pSTAT3	TYK2	66	16, 0.81	23	1.0x	2.4x	0.028x	1300	56x
3	IL-6-pSTAT3	JAK1	110	6.2, 0.81	2.9	26x	39x	10x	210	71x
4	IL-6-pSTAT3	JAK1	9	3.6, 0.80	0.89	2.7x	ⁱ 16x	^j 18x	45	50x
5	IL-6-pSTAT3	JAK1	53	3.4, 1.2	0.64	1.1x	0.50x	11x	39	61x

^aCell-based data for each compound was obtained from the indicated references: 1⁷, 2⁸, 3⁹, 4¹⁰, 5⁹.

^bSee Supplementary Data for assay details.

^cPermeability in transwell MDCK assays. Units: cm/s x 10⁻⁶. A:B classifications: <1 = low, 1 – 10 = moderate, >10 = high.

^dBiochemical JAK1 K_i . Genentech assay.

^eRatio of biochemical JAK2 K_i / JAK1 K_i . Genentech assays.

^fRatio of biochemical JAK3 K_i / JAK1 K_i . Genentech assays unless otherwise indicated.

^gRatio of biochemical TYK2 K_i / JAK1 K_i . Genentech assays unless otherwise indicated.

^hBiochemical to cell shift from the JAK1 biochemical assays to the IL-13-pSTAT6 cell-based assay.

ⁱRatio of biochemical JAK3 IC_{50} / JAK1 IC_{50} . SelectScreen Kinase Profiling Services, Thermo Fisher Scientific, Madison, WI.

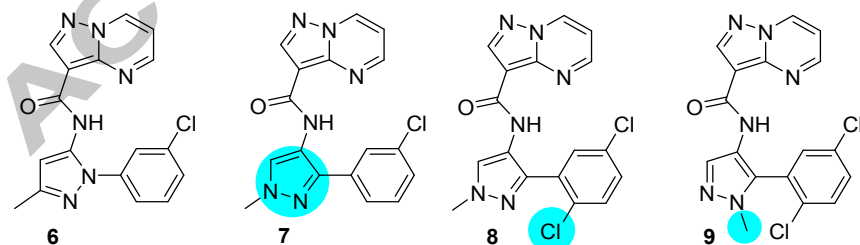
^jRatio of biochemical TYK2 IC_{50} / JAK1 IC_{50} . SelectScreen Kinase Profiling Services, Thermo Fisher Scientific, Madison, WI.

^k IC_{50} not reported since 50% inhibition not achieved at top concentration tested (1 μ M).

^lNot calculated since an IL-13-pSTAT6 IC_{50} was not reported.

Genentech has previously disclosed a series of pyrazolopyrimidine JAK inhibitors.¹² Although optimized to be most potent against JAK2, these compounds retained residual levels of JAK1 inhibition. Selected SAR highlights are shown in Table 2. The JAK potency of an early example (**6**) was improved by incorporating a regioisomeric central pyrazole moiety (**7**). Further elaboration with a 2,5-dichlorophenyl group (**8**) led to additional JAK potency enhancement. Translocation of the methyl group to the alternate N of the central pyrazole (**9**) was deleterious to potency. Consistent with the data generated with the compounds in Table 1, the relatively weak JAK1 biochemical potencies of compounds **7**, **8**, and **9** resulted in correspondingly weak cell-based disruption of IL-13 signaling. In order to more effectively block IL-13 signaling, we wished to discover related analogs with improved JAK1 inhibition.

^a**Table 2.** Biochemical and cell-based JAK inhibition of previously reported¹² pyrazolopyrimidine JAK inhibitors.



Ex	^b JAK1 K_i (nM)	^b JAK2 K_i (nM)	^b IL-13- pSTAT6 IC_{50} (nM)
----	---------------------------------	---------------------------------	---

6	110	12	
7	46	6.4	>1000
8	2.8	0.42	230
9	39	3.5	>1000

^aBlank space indicates data not generated.

^bGenentech assays. All values represent the mean of at least two independent runs. See Supplementary Data for assay details.

To generate hypotheses for additional JAK1 potency optimization we examined JAK-complexed crystal structures of ADP¹³, and compound **6**.¹² As expected, ADP forms multiple favorable interactions with JAK1, including engaging Glu966 and Arg1007 in hydrogen bond (H-bond) interactions via the ribose hydroxyl groups (Figure 1a). The binding mode of compound **6** relative to ADP is shown in Figure 1b, and these structures guided further optimization of compound **8**. For example, as shown in Figure 1c, appropriate substitution at positions R¹ and R² could offer productive vectors to engage Glu966 and Arg1007.

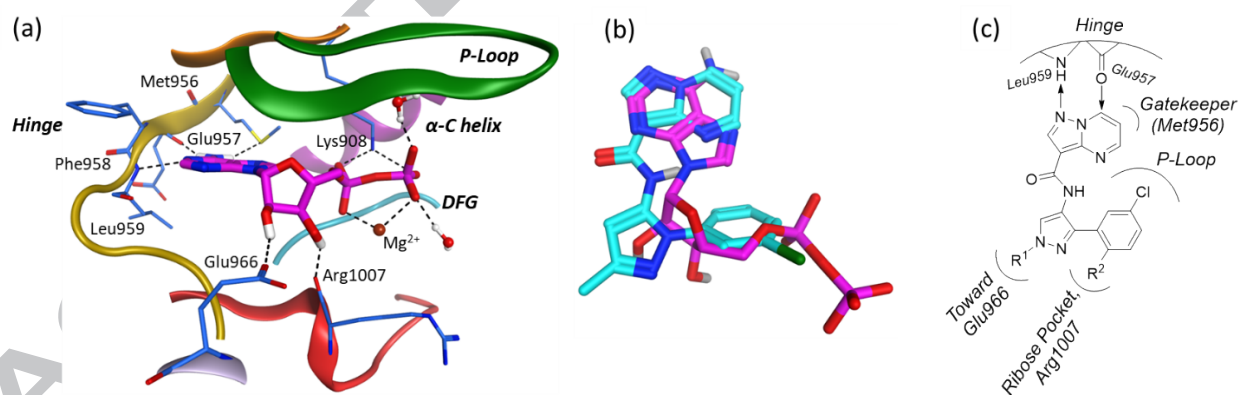


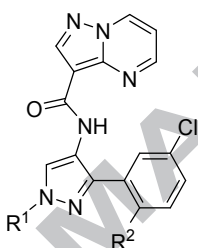
Figure 1. X-ray crystal structures (a) ADP bound to JAK1 (PDB Accession code: 5KHW¹³). (b) Overlay of ADP and **6**. Ligands extracted from PDB Accession codes: 5KHW¹³ and 4HGE¹². (c) Binding mode of pyrazolopyrimidine scaffold in JAK1.

Since substitutions at R¹ and R² were expected to approach Glu966 and Arg1007, respectively, we wished to study whether modifications at those positions would impact JAK1 potency (Table 3). Additionally, since compound **8** was already a relatively lipophilic starting point we wished to improve potency while maintaining or lowering cLogP. Excessive cLogP is linked to a number of undesirable properties such as promiscuity and toxicity, thus lipophilic ligand efficiency (LLE) was used as a convenient metric to optimize for maximum potency with minimum cLogP.¹⁴ Analogs **10** – **12** (Table 3) were synthesized in an attempt to engage Arg1007 with a H-bond, but a large JAK1 potency loss was observed in each case relative to **8**. Analogs **13** – **23** were designed to optimally fill the ribose pocket by substituting at R². Notably, JAK1 potency and LLE could be significantly improved by appropriate substitution at R² into the ribose pocket. For example, compound **15** was ~4.5-fold more potent against JAK1 than compound **8** with a substantial improvement in LLE. Groups larger than the methyl ether present in **15** were generally not beneficial to potency (compounds **16** – **19**). However, incorporation of a difluoromethoxy group was a notable exception, with compounds **20** and **21** exhibiting improved biochemical and cell-based potency relative to their methoxy matched pairs **14** and **15**. Although not immediately obvious, x-ray crystal structures ultimately revealed that the difluoromethoxy group not only optimally filled the ribose pocket, but also engaged Arg1007 in a H-bonding interaction (see Figures 2c and 2d). The final ribose pocket modifications surveyed were analogs **22** and **23**. Although the thiomethyl ether **22** was more potent than its methyl ether matched pair **15**, potency was not further improved by incorporation of the difluoromethyl moiety (compound

23). Thus, the difluoromethoxy R² group was chosen as the favored substitution for further SAR exploration.

Several of the analogs in Table 3 (**14**, **16**, **17**, **19**, **20**, **23**) were designed to H-bond to Glu966 via the hydrogen atom at R¹ of the central pyrazole. However, despite the additional H-bond interaction (see Figure 2), potency was not significantly improved, as evidenced by the R¹ H→CH₃ matched pairs **14**→**15** and **20**→**21**.

^a**Table 3.** Influence of groups targeting ribose pocket / Arg1007 and Glu966 on biochemical and cell-based JAK inhibition.



Ex	R ¹	R ²	cLogP	^b JAK1 LLE	^c JAK1 K _i (nM)	^c JAK2 K _i (nM)	^c IL-13-pSTAT6 IC ₅₀ (nM)
8	CH ₃	Cl	3.1	5.5	2.8	0.42	230
10	CH ₃		2.1	5.4	32	13	
11	CH ₃		1.6	5.7	45	8.6	
12	CH ₃		2.0	5.9	12	4.0	
13	CH ₃		3.2	5.8	0.91	0.28	
14	H		2.2	6.9	0.89	0.36	23
15	CH ₃		2.3	6.9	0.57	0.35	25
16	H		2.6	6.3	1.4	0.80	54

17	H		2.8	6.1	1.3	0.45	21
18	CH ₃		3.1	5.0	7.9	2.0	
19	H		3.4	5.3	2.1	0.49	64
20	H		2.5	7.2	0.21	0.071	5.2
21	CH ₃		2.7	7.0	0.21	0.088	4.7
22	CH ₃		3.1	6.2	0.46	0.23	11
23	H		3.6	5.5	0.85	0.23	26

^aBlank spaces indicate data not generated.

^bLLE = JAK1 pK_i – cLogP

^cGenentech assays. All values represent the mean of at least two independent runs. See Supplementary Data for assay details.

Figure 2 summarizes x-ray structural observations related to key SAR described thus far. As expected from the JAK2 crystal structure of **6**¹², compounds **15**, **20**, and **21** bind via their pyrazolopyrimidine motifs to the JAK1 hinge residues Leu959 and Glu957, and interact with the gatekeeper Met956 sidechain (Figures 2b, 2c, 2d). The chlorophenyl group present in each of **15**, **20**, and **21** participates in favorable Van der Waals interactions with the JAK1 P-Loop. In the case of **15**, the phenyl methoxy group extends into the base of the ribose pocket and makes a favorable Van der Waals contact with the sidechain of Leu1010 (Figure 2b). As shown in Figure 2a, the x-ray crystal structures of compound **15**, and the more potent analogs **20** and **21**, are similar, with only a minor downward movement of the P-Loops and ligands observed for **20** and **21**. These subtle shifts are likely a result of the additional interactions observed between the difluoromethoxy groups present in **20** and **21** and the ribose pocket of the JAK1 protein. Similar

to the methoxy group present in **15** the potency-enhancing difluoromethoxy groups in **20** and **21** participate in favorable Van der Waals interactions with Leu1010. Additionally, **20** and **21** participate in favorable Van der Waals interactions with the sidechain methylene of Ser963, as well as dipolar interactions with the backbone carbonyl carbon of Gly1020 (both interactions via the fluorine atoms); while the polarized H resident in the difluoromethoxy group forms a non-classical hydrogen bond with the backbone carbonyl of Arg1007. Notably, ADP in complex with JAK1 was also observed to hydrogen bond with the Arg1007 backbone carbonyl (see Figure 1a). We believe these additional ribose pocket interactions are the source of the enhanced potency of the difluoromethoxy analogs **20** and **21** relative to the methoxy analogs **14** and **15**. A final important structural observation is the apparent lack of benefit of interacting with the sidechain of Glu966. Although ADP does form a hydrogen bond with the carboxylate sidechain of Glu966 (Figure 1a), this residue is solvent exposed and conformationally mobile (compare Figures 2b, 2c, and 2d). Thus, although **20** forms a hydrogen bond with Glu966 while compound **21** does not (Figure 2c vs. Figure 2d), the JAK1 potency of the two compounds is virtually identical.

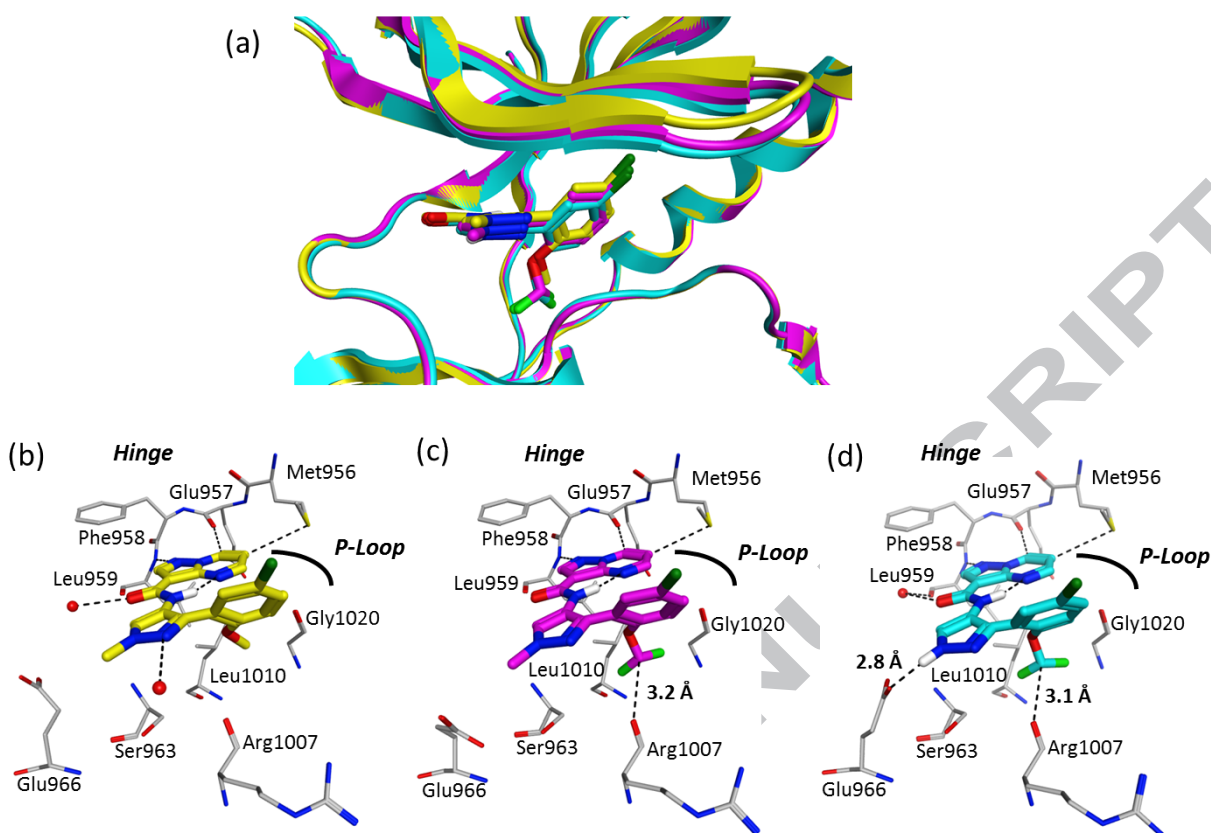
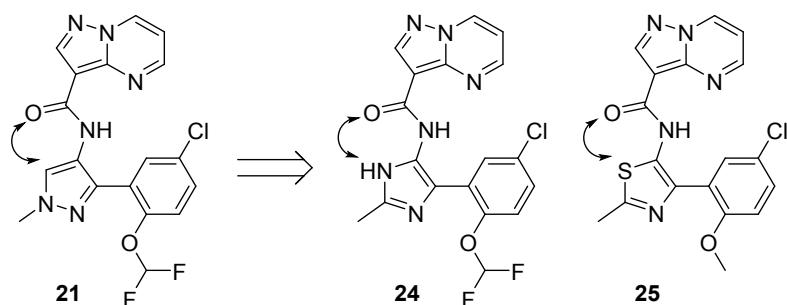


Figure 2. X-ray crystal structures of **15** (yellow), **21** (pink), and **20** (cyan) in complex with JAK1. (a) Overlay of all three structures. (b), (c), (d): Individual structures of **15** (PDB Accession code: 6N77), **21** (PDB Accession code: 6N78), and **20** (PDB Accession code: 6N79), respectively. Where indicated, distances refer to heavy atom to heavy atom.

Having optimized the ribose pocket group, we then surveyed additional heterocycles as potential replacements for the central pyrazole ring. The primary design hypothesis was to enforce the co-planarity between the central heterocycle and the proximal amide carbonyl with either a NH→O H-bond or related S→O interaction (see Table 4). Unfortunately, both imidazole **24** and thiazole **25** lost potency compared to the corresponding pyrazole **21**.

^a**Table 4.** Influence of central pyrazole replacements on biochemical and cell-based JAK inhibition.



Ex	cLogP	^b JAK1 LLE	^c JAK1 K_i (nM)	^c JAK2 K_i (nM)	^c IL-13-pSTAT6 IC ₅₀ (nM)
24	3.0	5.4	3.9	1.1	
25	3.1	5.9	0.99	0.45	58

^aBlank spaces indicate data not generated.

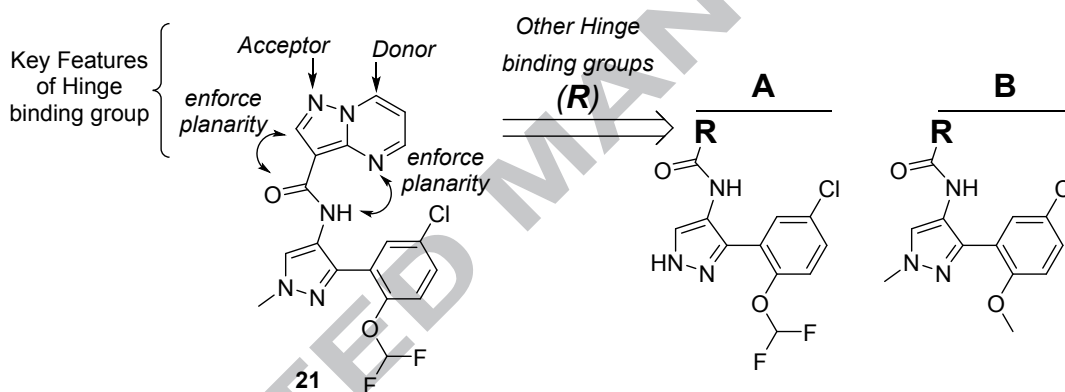
^bLLE = JAK1 p*K_i* – cLogP

^cGenentech assays. All values represent the mean of at least two independent runs.

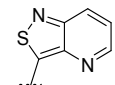
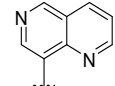
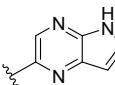
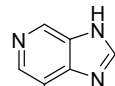
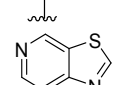
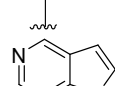
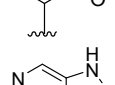
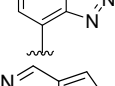
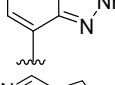
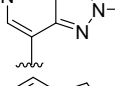
The next region of optimization was the bicyclic hinge binder. Table 5 summarizes the key hypotheses guiding design of the hinge binders, as well as SAR of the final compounds. Compounds **26** (extra hinge-binding contact) and **27** (regioisomeric hinge binder) were approximately equipotent to the matched pair **20**. Substitution on the 6-membered pyrimidine or pyridazine ring was detrimental to potency (**28 – 30**), as was incorporation of an isothiazolopyridine as the hinge binder (**31**). A 6,6-hinge binder was detrimental to potency (**32**), as were a number of related 6,5-systems (**33 – 37**). One promising alternate hinge binder was pyrazolopyridine **38** which displayed potency similar to the matched pair pyrazolopyrimidine **15**. Methylation of the hinge binding pyrazole moiety to enforce the tautomer required for an intramolecular H-bond with the pendant amide led to a loss in potency (**39**). Examination of crystal structures of pyrazolopyrimidine **15** and pyrazolopyridines **38** and **39** (Figure 3) reveals that the scaffolds bind to JAK1 with similar interactions to the hinge and gatekeeper residues,

and a virtually identical placement of the P-Loop and ribose pocket moieties. Notably, the pyrazole hinge binder moiety of **38** approaches within H-bonding distance (2.69 Å) to a crystallographic water molecule already tightly bound to Met956, Gly1020, and Asp1021 (Figure 3b). The methylated pyrazole hinge binder (**39**), while enforcing the low energy binding conformation, also disrupts the tightly bound crystallographic water, presumably leading to the loss in potency (Figure 3c). Incorporation of the difluoromethoxy ribose pocket group with the optimal 6,5 hinge binder led to a minor increase in potency (**38**→**40**).

^a**Table 5.** Influence of hinge-binding groups on biochemical and cell-based JAK inhibition.



Ex	A or B	R	cLogP	^b JAK1 LLE	^c JAK1 K_i (nM)	^c JAK2 K_i (nM)	^c IL-13-pSTAT6 IC ₅₀ (nM)
26	A		2.0	7.7	0.19	0.042	4.0
27	A		3.0	6.7	0.21	0.071	5.0
28	A		2.8	5.3	7.8	2.4	
29	A		2.9	6.1	0.99	0.10	34
30	A		3.3	6.2	0.29	0.078	13

31	A		3.0	6.3	0.47	0.085	20
32	B		2.8	5.9	1.9	0.62	38
33	A		2.9	5.3	5.6	0.96	42
34	B		2.3	5.9	5.7	2.6	
35	A		3.0	6.3	0.51	0.17	9.2
36	A		3.4	5.3	1.8	0.50	36
37	B		2.1	4.3	370	730	
38	B		2.0	7.2	0.60	0.78	20
39	B		2.1	6.3	4.3	4.7	93
40	A		2.2	7.1	0.56	0.49	18

^aBlank spaces indicate data not generated.

^bLLE = JAK1 pK_i - cLogP

^cGenentech assays. All values represent the mean of at least two independent runs. See Supplementary Data for assay details.

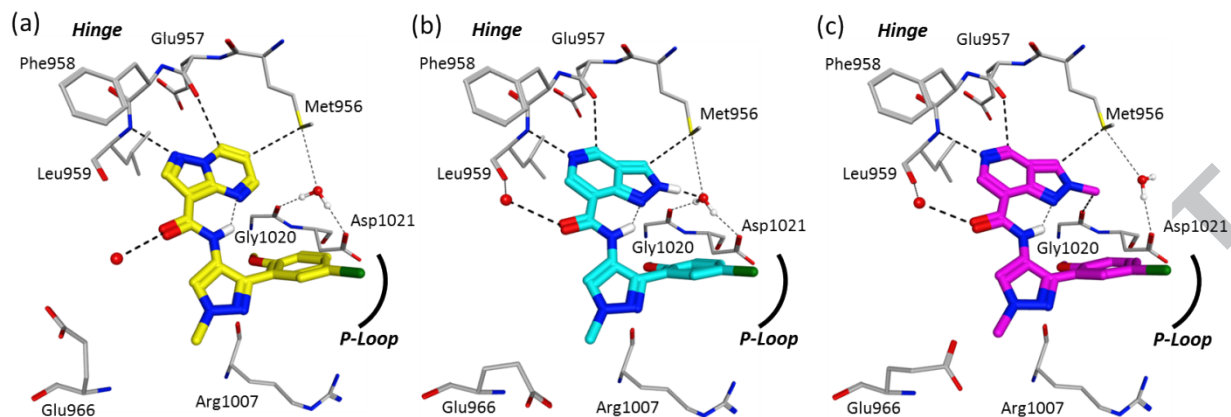


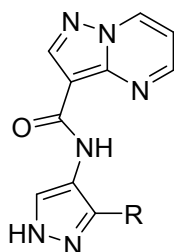
Figure 3. X-ray crystal structures of (a) **15** (PDB Accession code: 6N77), (b) **38** (PDB Accession code: 6N7B), and (c) **39** (PDB Accession code: 6N7A) in complex with JAK1.

As shown in Table 6, a final round of SAR exploration was conducted on the phenyl ring extending beneath the P-Loop (see compound **41** for numbering convention). Substitution at the 5-position of the phenyl was important (**41** – **47**), and the most lipophilic groups were typically most potent (**46**, **47**). Fluorine incorporation was not beneficial at the 6-position (**48**, **49**), and led to a potency loss at the 3- and 4-positions (**50**, **51**). Notably, however, installation of H-bond donors at the 4-position (**52** – **55**) led to highly biochemically potent compounds, with indazole **55** in particular displaying exceptional levels of biochemical JAK1 inhibition ($K_i = 75$ pM) and LLE (8.4). Despite the outstanding JAK1 biochemical potency, a large cell shift was observed for **55** presumably due to permeability limitations (see Table 8). Replacement of the indazole ring with a naphthalene moiety led to a reduction in biochemical potency, but a smaller cell shift (**56** and **57**). As a result, compound **57** exhibited biochemical and cell-based potency similar to compound **20**.

As shown in Figure 4, the chlorophenyl (**15**), indazole (**54**), and naphthyl (**56**) containing compounds bind in a similar orientation to JAK1 (Figure 4a), with a small degree of P-loop collapse around indazole **54** likely due to its smaller size. Additionally, the indazole participates

in a H-bonding interaction with the sidechain of Asp1021, likely leading to the increase in LLE and biochemical JAK1 inhibition (Figure 4b). By comparison, the naphthyl group does not make any specific H-bonds and, as suggested by its lower LLE, its affinity is driven by hydrophobic interactions (Figure 4c).

^a**Table 6.** Influence of P-Loop groups on biochemical and cell-based JAK inhibition.



Ex	R	cLogP	^b JAK1 LLE	^c JAK1 K_i (nM)	^c JAK2 K_i (nM)	^c IL-13-pSTAT6 IC_{50} (nM)
41		1.8	6.7	3.3	0.86	
42		1.5	7.5	0.90	0.27	22
43		2.0	7.1	0.71	0.19	34
44		2.2	6.6	1.4	0.34	27
45		2.6	6.7	0.53	0.19	13

46		2.8	7.1	0.12	0.047	3.3
47		3.0	6.8	0.15	0.045	2.8
48		2.2	6.8	0.95	0.29	15
49		3.0	6.3	0.56	0.16	14
50		2.3	5.7	9.2	1.2	
51		2.2	6.5	2.2	0.79	42
52		1.8	7.7	0.31	0.16	140
53		2.1	7.9	0.11	0.057	36
54		1.3	8.2	0.30	0.20	370
55		1.7	8.4	0.075	0.052	40
56		2.6	6.6	0.67	0.34	14
57		3.0	6.5	0.31	0.14	6.4

^aBlank spaces indicate data not generated.

^bLLE = JAK1 pK_i - cLogP

°Genentech assays. All values represent the mean of at least two independent runs. See Supplementary Data for assay details.

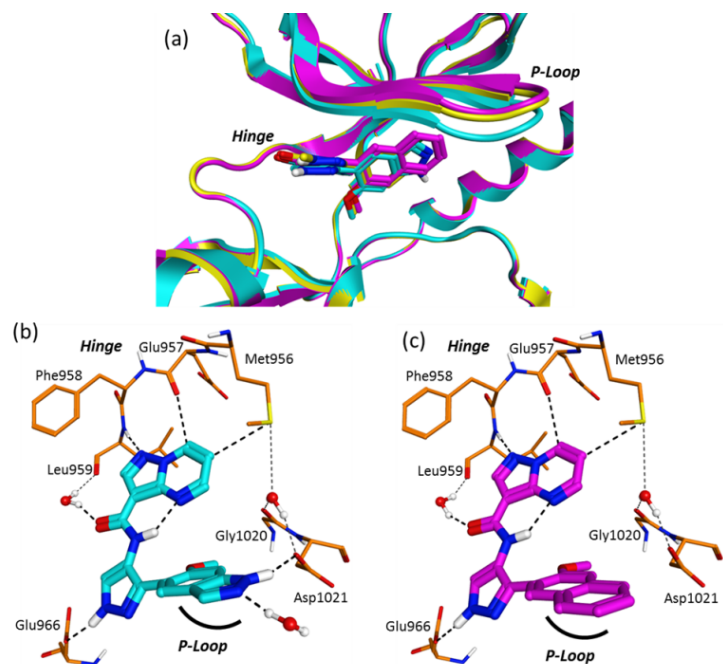


Figure 4. X-ray crystal structures of **15** (yellow), **54** (cyan), and **56** (pink) in complex with JAK1. (a) Overlay of all three structures. (b), (c): Individual structures of **54** (PDB Accession code: 6N7D), and **56** (PDB Accession code: 6N7C), respectively.

To assess selectivity for the JAK family relative to off-target kinases we screened several optimized inhibitors against a panel of kinases. As shown in Figure 5, compound **20** was found to be relatively selective for the JAK family, with LRRK2 and FYN being the only non-JAK kinases significantly inhibited in a 71-membered panel. LRRK2 was believed to be an off-target kinase of concern since potent inhibition has been implicated in lung toxicity.¹⁵ In an effort to identify compounds with reduced LRRK2 potency, multiple analogs were screened against LRRK2 at a single concentration of 0.1 μM , with a smaller number of compounds subsequently advanced to a detailed selectivity measurement comparing the LRRK2 IC_{50} relative to the JAK1 IC_{50} (Table 7). In determining the selectivity for JAK1 relative to LRRK2 we believed it was important to use the same assay format for both assays. Since the LRRK2 assay was conducted

Ex	^b % LRRK2 Inhibition @ 0.1 μ M	^b LRRK2 IC ₅₀ (nM)	^b JAK1 IC ₅₀ (nM)	LRRK2 IC ₅₀ \div JAK1 IC ₅₀
8	14	400	32	13x
20	87	18	1.2	15x
21	61	81	1.7	47x
26	99			
40	52	79	1.9	41x
46	86			
47	91			
55	89			
57	31	180	2.2	83x

^aBlank spaces indicate data not generated.

^bSelectScreen Kinase Profiling Services, Thermo Fisher Scientific, Madison, WI. See Supplementary Data for assay details.

Finally, the majority of compounds were found to have moderate to poor metabolic stability when incubated with human liver microsomes (Table 8). The only metabolically stable example was **55**, a molecule with a markedly lower LogD_{7.4} than the other compounds in Table 8. Unfortunately, **55** also possessed dramatically reduced membrane permeability as measured in MDCK transwell assays, leading to impaired cell potency (see Table 6) and concern that it would suffer from permeability-limited intestinal absorption if dosed orally. This series of compounds may, thus, be most suited for optimization as locally delivered topical agents, where poor metabolic stability is a desirable feature.

Table 8. Metabolic stability, lipophilicity, and permeability of selected analogs.

Ex	^a HLM CL	^b LogD _{7.4}	^c MDCK A:B, B:A÷A:B
8	12	2.9	20, 0.88
20	14	3.2	14, 1.1
21	15	3.0	14, 0.55
26	11	3.3	15, 0.83
40	15	2.7	9.5, 1.9
46	15	3.2	17, 1.2
47	15	3.4	15, 1.0
55	4.4	1.6	1.6, 1.0
57	17	3.5	13, 1.2

^aClearance predicted from human liver microsomes. Units: mL/min/kg. See Supplementary Data for assay details.

^bMeasured LogD_{7.4}.¹⁷

^cPermeability in transwell MDCK assays. Units: cm/s x 10⁻⁶. See Supplementary Data for assay details. A:B classifications: <1 = low, 1 – 10 = moderate, >10 = high.

In conclusion, a series of highly potent JAK1/2 inhibitors has been identified. Notably, the significantly improved JAK1 potency also led to effective blockade of cell-based IL-13 signaling. Compounds **21** and **57** showed an optimum balance between potent JAK1 inhibition and minimal off target kinase inhibition. All of the analogs exhibiting the best cell-based potency were also found to be poorly stable in the presence of human liver microsomes. Exquisite potency, favorable kinome selectivity, and metabolic lability are preferred features in compounds intended for local delivery as topical agents. Given IL-13's role in diseases of the lungs and skin², additional optimization of this series for topical delivery to those organs may be warranted.

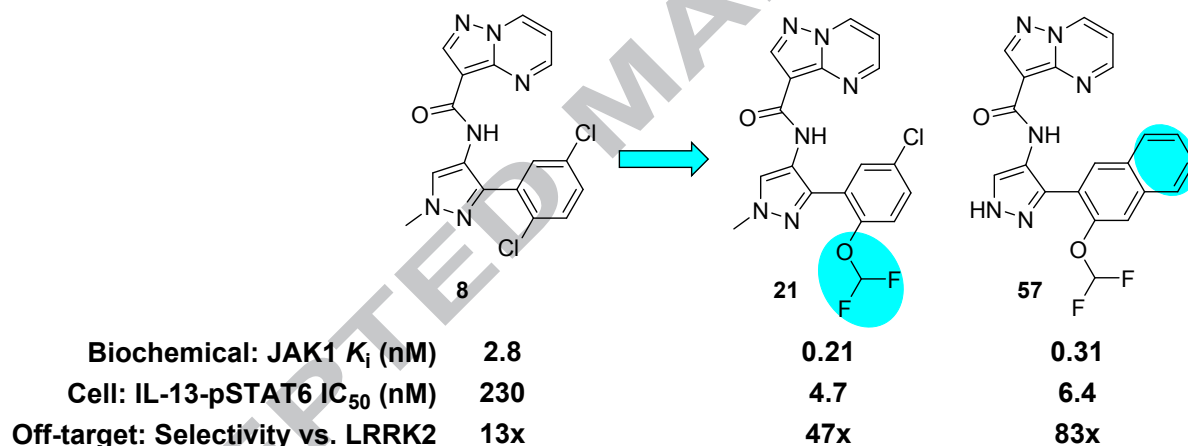
Appendix A. Supplementary Data

Experimental procedures and analytical data for compounds **20** and **21**. Synthetic schemes and general reaction conditions for all compounds **10-57**. Crystallography statistics for compounds **15**, **20**, **21**, **38**, **39**, **54**, and **56** in complex with JAK1. Procedures for Genentech biochemical and cell-based assays, and Thermo Fisher biochemical kinase assays. Procedures for MDCK and liver microsome stability assays.

Acknowledgements

This work was funded by Genentech.

References and Notes



¹ Shuai K, Liu B. Regulation of JAK-STAT signalling in the immune system. *Nat Rev Immunol*. 2003;3(11): 900-911.

² (a) Wills-Karp M, Luyimbazi J, Xu X, et al. Interleukin-13: Central Mediator of Allergic Asthma. *Science*. 1998;282(5397): 2258-2261. DOI: 10.1126/science.282.5397.2258. (b) Corren J. Role of interleukin-13 in asthma. *Curr Allergy Asthma Rep*. 2013;13(5): 415-420. DOI: 10.1007/s11882-013-0373-9. (c) Wollenberg A, Howell MD, Guttman-Yassky E, et al. Treatment of atopic dermatitis with tralokinumab, an anti-IL-13 mAb. *J Allergy Clin Immunol*. 2018. DOI: 10.1016/j.jaci.2018.05.029. (d) Simpson EL, Flohr C, Eichenfield LF, et al. Efficacy

and safety of lebrikizumab (an anti-IL-13 monoclonal antibody) in adults with moderate-to-severe atopic dermatitis inadequately controlled by topical corticosteroids: A randomized, placebo-controlled phase II trial (TREBLE). *J Am Acad Dermatol*. 2018;78(5): 863-871 e811. DOI:10.1016/j.jaad.2018.01.017.

³ Clark JD, Flanagan ME, Telliez JB. Discovery and development of Janus kinase (JAK) inhibitors for inflammatory diseases. *J Med Chem*. 2014;57(12): 5023-5038. DOI: 10.1021/jm401490p.

⁴ Sohn SJ, Barrett K, Van Abbema A, et al. A restricted role for TYK2 catalytic activity in human cytokine responses revealed by novel TYK2-selective inhibitors. *J Immunol*. 2013;191(5): 2205-2216. DOI: 10.4049/jimmunol.1202859.

⁵ Reddel RR, Ke Y, Gerwin BI, et al. Transformation of Human Bronchial Epithelial Cells by Infection with SV40 or Adenovirus-12 SV40 Hybrid Virus, or Transfection via Strontium Phosphate Coprecipitation with a Plasmid Containing SV40 Early Region Genes. *Cancer Research*. 1988;48(7): 1904-1909.

⁶ Details on the IL-13-pSTAT6 assay may be found in the Supplementary Data section.

⁷ Wan H, Schroeder GM, Hart AC, et al. Discovery of a Highly Selective JAK2 Inhibitor, BMS-911543, for the Treatment of Myeloproliferative Neoplasms. *ACS Med Chem Lett*. 2015;6(8): 850-855. DOI: 10.1021/acsmchemlett.5b00226.

⁸ Liang J, Van Abbema A, Balazs M, et al. Identification of an imidazopyridine scaffold to generate potent and selective TYK2 inhibitors that demonstrate activity in an in vivo psoriasis model. *Bioorg Med Chem Lett*. 2017;27(18): 4370-4376. DOI: 10.1016/j.bmcl.2017.08.022.

⁹ Zak M, Hurley CA, Ward SI, et al. Identification of C-2 hydroxyethyl imidazopyrrolopyridines as potent JAK1 inhibitors with favorable physicochemical properties and high selectivity over JAK2. *J Med Chem*. 2013;56(11): 4764-4785. DOI: 10.1021/jm4004895.

¹⁰ WO2015061665. Jak1 selective inhibitor and uses thereof. Voss JW, Camp HS, Padley RJ.

¹¹ Flanagan ME, Blumenkopf TA, Brissette WH, et al. Discovery of CP-690,550: a potent and selective Janus kinase (JAK) inhibitor for the treatment of autoimmune diseases and organ transplant rejection. *J Med Chem*. 2010;53(24): 8468-8484.

¹² Hanan EJ, van Abbema A, Barrett K, et al. Discovery of potent and selective pyrazolopyrimidine janus kinase 2 inhibitors. *J Med Chem*. 2012;55(22): 10090-10107. DOI: 10.1021/jm3012239.

¹³ Caspers NL, Han S, Rajamohan F, et al. Development of a high-throughput crystal structure-determination platform for JAK1 using a novel metal-chelator soaking system. *Acta Crystallogr F Struct Biol Commun*. 2016;72(Pt 11): 840-845. DOI: 10.1107/S2053230X16016356.

¹⁴ Freeman-Cook KD, Hoffman RL, Johnson TW. Lipophilic efficiency: the most important efficiency metric in medicinal chemistry. *Future Medicinal Chemistry*. 2013;5(2): 113-115. DOI: 10.4155/FMC.12.208

¹⁵ Fuji RN, Flagella M, Baca M, et al. Effect of selective LRRK2 kinase inhibition on nonhuman primate lung. *Science Translational Medicine*. 2015;7(273): 273ra15. DOI: 10.1126/scitranslmed.aaa3634.

¹⁶ Thermo Fisher JAK3 and TYK2 IC₅₀ values for **21** and **57** were also determined to enable selectivity calculations relative to JAK1. The following selectivity ratios were measured. Compound **21**: JAK3 IC₅₀ ÷ JAK1 IC₅₀ = 2.1x. TYK2 IC₅₀ ÷ JAK1 IC₅₀ = 3.0x. Compound **57**: JAK3 IC₅₀ ÷ JAK1 IC₅₀ = 2.7x. TYK2 IC₅₀ ÷ JAK1 IC₅₀ = 5.9x.

¹⁷ Lin B, Pease JH. A novel method for high throughput lipophilicity determination by microscale shake flask and liquid chromatography tandem mass spectrometry. *Comb. Chem. High Throughput Screen*. 2013;16(10): 817-825. DOI: 10.2174/1386207311301010007.

ACCEPTED MANUSCRIPT